

The Effect of Rotation on Thermoelastic Microelongated Medium under DPL Model

Mohamed I. A. Othman^{1,*}, Sarhan Y. Atwa², E. E. M. Eraki¹, Mohamed F. Ismail²

¹Department of Mathematics, Faculty of Science, Zagazig University, P.O. Box 44519, Zagazig, Egypt.

²Department of Engineering Mathematics and Physics, Higher Institute of Engineering, El Shorouk Academy, P.O. Box 11837, Egypt.

How to cite this paper: Mohamed I. A. Othman, Sarhan Y. Atwa, E. E. M. Eraki, Mohamed F. Ismail. (2023) The Effect of Rotation on Thermoelastic Microelongated Medium under DPL Model. *Journal of Applied Mathematics and Computation*, 7(1), 1-14.
DOI: 10.26855/jamc.2023.03.001

Received: December 22, 2022

Accepted: January 18, 2023

Published: February 13, 2023

***Corresponding author:** Mohamed I. A. Othman, Department of Mathematics, Faculty of Science, Zagazig University, P.O. Box 44519, Zagazig, Egypt.
Email: m_i_a_othman@yahoo.com

Abstract

The effect of rotation on a two-dimensional micro-elongated thermoelastic medium problem was studied under the dual-phase-lag (DPL) model. Mechanical force along with the layer of the elastic half-space interface and micro-elongated thermoelastic half-space is applied. The analytical method used was the normal mode which Partial differential equations transform into ordinary differential equations. The analytic expressions for displacement component, temperature distribution, micro-elongational scalar and stress components have been derived and represented graphically. The work in its present form has not been studied by any researcher till now. The novelty of the present article resides in the fact that we have proposed a new research problem to study the effect of rotation on the physical quantities in the context of the Lord-Shulman theory and the DPL model. The problem is pretty important in many dynamical systems.

Keywords

Thermoelasticity, Micro-Elongation, Rotation, Normal Mode, Elastic Solid

1. Introduction

In the generalized theories, the governing equations involve thermal relaxation times and they are of a hyperbolic type. The extended thermoelasticity theory by [1-5] which introduces one relaxation time in the thermoelastic process and the temperature-rate dependent theory of thermoelasticity by [6], which takes into account two relaxation times are two well-established generalized theories of thermoelasticity.

A micro-elongated elastic solid possesses four degrees of freedom: three for translation and micro-elongation. In micro-elongation theory, the material particles can perform only volumetric micro-elongation in addition to classical deformation of the medium. The material points of such a medium can stretch and contract independently of their translations. Solid-liquid crystals, composite materials reinforced with chopped elastic fibers porous media with pores filled with non-viscous fluid or gas can be categorized as micro-elongated medium. The variation of periodical heat source response in a functionally graded micro-elongated medium was discussed by [7, 8]. The plane strain problem in a thermoelastic micro-elongated solid with an overlying infinite non-viscous fluid was discussed by [9]. More interesting problems have been studied about the thermoelastic micro-elongated solid in different cases [10-17].

A new model called the dual-phase-lag model for the heat transport mechanism in which Fourier's law is replaced by an approximation to the modification of Fourier's law with two different time translations for the heat flux and the temperature gradient was developed by [18-22]. The effect of thermal loading due to laser pulse in generalized thermoelastic medium with voids in the dual-phase-lag model was studied by [23]. A dynamic problem in thermoelastic solid using a dual-phase-lag model with an internal heat source was explained by [24]. The effect of rotation on micropolar generalized

thermoelasticity with two-temperatures and the thermal laser pulse using a DPL model has been discussed by [25, 26].

The current manuscript is an attempt to study the influence of rotation on a two-dimensional micro-elongated thermoelastic medium problem. The normal mode analysis is used to derive the expressions for the considered variables for a DPL model of thermoelasticity and the variances of the considered variables are represented graphically.

2. Formulation of the Problem

The system of governing equations of a micro-elongated thermoelasticity with rotation, in a DPL model, can be written as [10, 13] (Fig. 1)

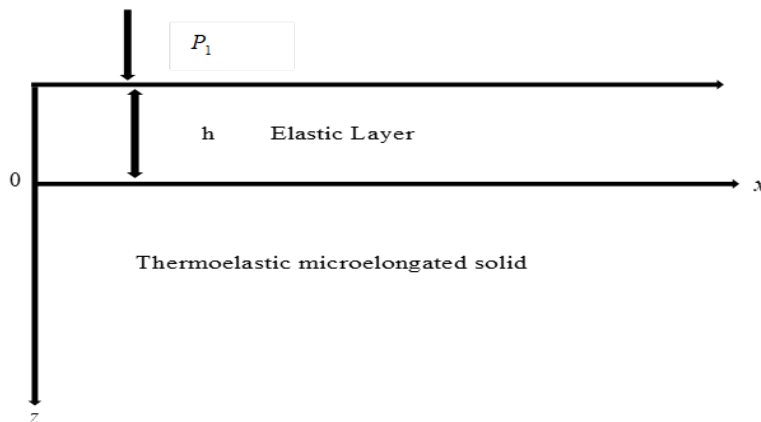


Figure 1. Geometry of the problem.

$$\sigma_{ij,j} = \rho [u_{i,tt} + \{\Omega \times (\Omega \times u)\}_i + (2\Omega \times u_{,t})_i], \tag{1}$$

$$a_0 \varphi_{,ii} + \beta_1 T - \lambda_1 \varphi - \lambda_0 u_{j,j} = \frac{1}{2} \rho j_0 \varphi_{,tt}, \tag{2}$$

$$k (1 + \tau_\theta \frac{\partial}{\partial t}) T_{,ii} = (1 + \tau_q \frac{\partial}{\partial t}) (\rho c_e \frac{\partial T}{\partial t} + \beta_0 T u_{k,kt}) + \beta_1 T_0 \varphi_{,t}, \tag{3}$$

$$\sigma_{ij} = 2\mu \varepsilon_{ij} + (\lambda e - \beta_0 T + \lambda_0 \varphi) \delta_{ij}. \tag{4}$$

From Eqs. (1) - (4) for displacement vector $\mathbf{u}(x, z, t) = u(u_1, 0, u_3)$, and the rotation $\Omega = (0, \Omega, 0)$ the equations of motion are given by

$$\mu \nabla^2 u_1 + (\lambda + \mu) e_{,x} - \beta_0 T_{,x} + \lambda_0 \varphi_{,x} = \rho (u_{1,tt} - \Omega^2 u_1 + 2\Omega u_{3,t}), \tag{5}$$

$$\mu \nabla^2 u_3 + (\lambda + \mu) e_{,z} - \beta_0 T_{,z} + \lambda_0 \varphi_{,z} = \rho (u_{3,tt} - \Omega^2 u_3 + 2\Omega u_{1,t}). \tag{6}$$

For simplification, we shall use the following non-dimensional variables

$$x'_i = \frac{w^*}{c_1} x_i, \quad z' = \frac{w^*}{c_1} z, \quad u'_i = \frac{w^* \rho c_1}{\beta_0 T_0} u_i, \quad u'^e_i = \frac{w^* \rho c_1}{\beta_0 T_0} u^e_i, \quad t' = w^* t, \quad \tau'_\theta = w^* \tau_\theta, \quad \tau'_q = w^* \tau_q, \tag{7}$$

$$\sigma'_{ij} = \frac{\sigma_{ij}}{\beta_0 T_0}, \quad \sigma'^e_{ij} = \frac{\sigma^e_{ij}}{\beta_0 T_0}, \quad \varphi' = \frac{\lambda_0}{\beta_0 T_0} \varphi, \quad T' = \frac{T}{T_0}, \quad \Omega' = \frac{\Omega}{w^*}, \quad P'_1 = \frac{P_1}{\beta_0 T_0}, \quad w^* = \frac{\rho c_1^2 c_e}{k},$$

$$c_1^2 = \frac{\lambda + 2\mu}{\rho}.$$

The displacement potentials $\Phi(x, z, t)$ and $\Psi(x, z, t)$ which relate to displacement components have been in-

roduced, we obtain

$$u_1 = \Phi_{,x} + \psi_{,z}, \quad u_3 = \Phi_{,z} - \psi_{,x}. \tag{8}$$

Substituting from Eqs. (7) and (8) into Eqs. (2), (3), (5) and (6), we obtain

$$[(a_1 + a_2) \nabla^2 + \Omega^2 - \frac{\partial^2}{\partial t^2}] \Phi + 2\Omega \psi_{,t} - T + \varphi = 0, \tag{9}$$

$$-2\Omega \Phi_{,t} + (a_1 \nabla^2 + \Omega^2 - \frac{\partial^2}{\partial t^2}) \psi = 0, \tag{10}$$

$$-a_5 \nabla^2 \Phi + a_3 T + (\nabla^2 - a_4 - a_6 \frac{\partial^2}{\partial t^2}) \varphi = 0, \tag{11}$$

$$-a_8 (1 + \tau_q \frac{\partial}{\partial t}) \nabla^2 \Phi_{,t} + (1 + \tau_\theta \frac{\partial}{\partial t}) \nabla^2 T - a_7 (1 + \tau_q \frac{\partial}{\partial t}) T_{,t} - a_9 \varphi = 0. \tag{12}$$

3. Solution methodology

In the current section, normal mode analysis technique is employed, which the advantage of finding the exact solutions without any has assumed restrictions on the field variables. The physical variables under consideration can be decomposed in terms of normal modes in the following form:

$$[u_i, \varphi, T, \psi, \Phi, \sigma_{ij}, u_i^e, \sigma_{ij}^e](x, z, t) = [u_i^*, \varphi^*, T^*, \psi^*, \Phi^*, \sigma_{ij}^*, u_i^{e*}, \sigma_{ij}^{e*}](z) e^{(\omega t + i b x)}. \tag{13}$$

Where, ω is a complex constant, $i = \sqrt{-1}$, b is the wave number in the x direction.

Making use of expression (13) into Eqs. (9)-(12), one can obtain the following set of equations

$$(a_{10} D^2 + a_{11}) \Phi^* + 2\Omega \omega \psi^* - T^* + \varphi^* = 0, \tag{14}$$

$$-2\Omega \omega \Phi^* + (a_1 D^2 + a_{12}) \psi^* = 0, \tag{15}$$

$$(-a_5 D^2 + a_{13}) \Phi^* + a_3 T^* + (D^2 - a_{14}) \varphi^* = 0, \tag{16}$$

$$(-a_{17} D^2 + a_{18}) \Phi^* + (a_{16} D^2 - a_{19}) T^* - a_9 \omega \varphi^* = 0. \tag{17}$$

By applying the elimination procedure in the system of Eqs. (14) - (17), we get the following eight-order differential equation:

$$(D^8 - A D^6 + B D^4 - C D^2 + E) \{ \Phi^*(z), \psi^*(z), T^*(z), \varphi^*(z) \} = 0 \tag{18}$$

Where, the coefficients a_i, A, B, C, E and H_{in} are given in Appendix 1.

Eq. (18) can be factorized as:

$$(D^2 - k_1^2)(D^2 - k_2^2)(D^2 - k_3^2)(D^2 - k_4^2) \{ \Phi^*(z), \psi^*(z), T^*(z), \varphi^*(z) \} = 0. \tag{19}$$

Where, $k_n^2, (n = 1, 2, 3, 4)$ are roots of the characteristic equation of Eq. (19)

The general solutions of Eq. (19) bound as $(z \rightarrow \infty)$ can be represented as:

$$(\Phi^*, \psi^*, T^*, \varphi^*)(z) = \sum_{n=1}^4 (1, H_{1n}, H_{2n}, H_{3n}) M_n e^{-k_n z}. \tag{20}$$

Substituting from Eq. (20) into Eq. (8) we obtain the components of displacements.

$$u_1^*(z) = \sum_{n=1}^4 (ib - k_n H_{1n}) M_n e^{-k_n z}, \tag{21}$$

$$u_3^*(z) = \sum_{n=1}^4 -(k_n + ib H_{1n}) M_n e^{-k_n z}. \tag{22}$$

Substituting Eqs. (7) and (13) into (4) and with the help of Eqs. (20)-(22) we obtain the components of stresses.

$$(\sigma_{xx}^*, \sigma_{zz}^*, \sigma_{xz}^*)(z) = \sum_{n=1}^4 (H_{4n}, H_{5n}, H_{6n}) M_n e^{-k_n z}, \tag{23}$$

The equations of motion and stress components in an elastic medium are given by [13]:

$$\sigma_{ij,j}^e = \rho^e u_{i,t}^e, \tag{24}$$

$$\sigma_{ij}^e = \lambda^e u_{k,k}^e \delta_{ij} + \mu^e (u_{i,j}^e + u_{j,i}^e). \tag{25}$$

Substituting from Eqs. (7) and (13) into Eq. (24)

$$(l_3 D^2 - \delta_1) u_1^{e*} + i b l_2 D u_3^{e*} = 0, \tag{26}$$

$$i b l_2 D u_1^{e*} + (l_1 D^2 - \delta_2) u_3^{e*} = 0. \tag{27}$$

Eliminating u_1^{e*}, u_3^{e*} between Eqs. (26) and (27), We obtain

$$(D^4 - G D^2 + N) \{u_1^{e*}(z), u_3^{e*}(z)\} = 0 \tag{28}$$

Eq. (28) can be factorized as:

$$(D^2 - r_1^2)(D^2 - r_2^2) \{u_1^{e*}(z), u_3^{e*}(z)\} = 0. \tag{29}$$

Where, $r_n^2, (n = 1, 2)$ are roots of the characteristic equation of Eq. (29), the solutions of Eq. (29) are of the form:

$$u_1^{e*}(z) = \sum_{n=1}^2 R_n e^{-r_n z} + \sum_{n=1}^2 R_{n+2} e^{r_n z}, \tag{30}$$

$$u_3^{e*}(z) = \sum_{n=1}^2 L_{1n} R_n e^{-r_n z} + \sum_{n=1}^2 L_{1(n+2)} R_{n+2} e^{r_n z}. \tag{31}$$

Substituting from Eqs. (7) and (13) into (25) and with the help of Eqs. (30) and (31), we obtain the components of stresses in an elastic medium

$$\sigma_{xx}^{e*}(z) = \sum_{n=1}^2 L_{2n} R_n e^{-r_n z} + \sum_{n=1}^2 L_{2(n+2)} R_{n+2} e^{r_n z}, \tag{32}$$

$$\sigma_{zz}^{e*}(z) = \sum_{n=1}^2 L_{3n} R_n e^{-r_n z} + \sum_{n=1}^2 L_{3(n+2)} R_{n+2} e^{r_n z}, \tag{33}$$

$$\sigma_{xz}^{e*}(z) = \sum_{n=1}^2 L_{4n} R_n e^{-r_n z} + \sum_{n=1}^2 L_{4(n+2)} R_{n+2} e^{r_n z}. \tag{34}$$

Where, the coefficients l_i, δ_i, G, N and L_m are given in Appendix 2.

4. Applications

The parameters $M_n, (n=1,2,3,4)$ and $R_n, (n=1,2,3,4)$ have to be selected such that boundary conditions at the surface are [9-13]

$$\begin{aligned} \sigma_{zz} = \sigma_{zz}^e, \quad \sigma_{xz} = \sigma_{xz}^e, \quad u_1 = u_1^e, \quad u_3 = u_3^e, \quad \varphi = 0, \quad \frac{\partial T}{\partial z} = 0, \quad \text{at } z = 0 \\ \sigma_{zz} = \sigma_{zz}^e - P_1 e^{(\omega t + i b x)}, \quad \sigma_{xz} = 0, \quad \text{at } z = -h. \end{aligned} \quad (35)$$

Where, P_1 is the magnitude of the mechanical force.

The utilization of the expressions of the variables considered into the previous boundary conditions (35), to obtain the equations that are satisfied with the parameters. And hence, eight equations will be obtained. If the inverse method matrix is applied to the eight equation, we get then the value constant $M_n, (n=1,2,3,4)$ and $R_n, (n=1,2,3,4)$

$$\begin{pmatrix} M_1 \\ M_2 \\ M_3 \\ M_4 \\ R_1 \\ R_2 \\ R_3 \\ R_4 \end{pmatrix} = \begin{pmatrix} H_{51} & H_{52} & H_{53} & H_{54} & -L_{31} & -L_{32} & -L_{33} & -L_{34} \\ H_{61} & H_{62} & H_{63} & H_{64} & -L_{41} & -L_{42} & -L_{43} & -L_{44} \\ ib - k_1 H_{11} & ib - k_2 H_{12} & ib - k_3 H_{13} & ib - k_4 H_{14} & -1 & -1 & -1 & -1 \\ -k_1 - ib H_{11} & -k_2 - ib H_{12} & -k_3 - ib H_{13} & -k_4 - ib H_{14} & -L_{11} & -L_{12} & -L_{13} & -L_{14} \\ H_{31} & H_{32} & H_{33} & H_{34} & 0 & 0 & 0 & 0 \\ -k_1 H_{21} & -k_2 H_{22} & -k_3 H_{23} & -k_4 H_{24} & 0 & 0 & 0 & 0 \\ H_{51} e^{k_1 h} & H_{52} e^{k_2 h} & H_{53} e^{k_3 h} & H_{54} e^{k_4 h} & -L_{31} e^{r_1 h} & -L_{32} e^{r_2 h} & -L_{33} e^{-r_1 h} & -L_{34} e^{-r_2 h} \\ H_{61} e^{k_1 h} & H_{62} e^{k_2 h} & H_{63} e^{k_3 h} & H_{64} e^{k_4 h} & 0 & 0 & 0 & 0 \end{pmatrix}^{-1} \begin{pmatrix} 0 \\ 0 \\ 0 \\ 0 \\ 0 \\ 0 \\ -P_1 \\ 0 \end{pmatrix} \quad (36)$$

5. Numerical results and analysis

The analysis is conducted for aluminum epoxy-like material as [26]:

$$\begin{aligned} \lambda = 7.59 \times 10^{10} \text{ N/m}^2, \quad \mu = 1.89 \times 10^{10} \text{ N/m}^2, \quad a_0 = 0.61 \times 10^{-10} \text{ N}, \quad \rho = 2.19 \times 10^3 \text{ kg/m}^3, \\ \beta_0 = \beta_1 = 0.05 \times 10^5 \text{ N/m}^2 \cdot \text{k}, \quad c_e = 966 \text{ J/kg} \cdot \text{k}, \quad k = 252 \text{ J/m} \cdot \text{s} \cdot \text{k}, \quad j_0 = 0.196 \times 10^{-4} \text{ m}^2, \\ \lambda_0 = \lambda_1 = 0.37 \times 10^{10} \text{ N/m}^2, \quad T_0 = 293 \text{ k}, \quad \tau_\theta = 0.02 \text{ s}, \quad \tau_q = 0.5 \text{ s}, \quad \omega = \omega_0 + i \zeta, \quad \omega_0 = 3.56, \\ \zeta = -4.81, \quad b = 8, \quad h = 1 \times 10^{-6}. \end{aligned}$$

The physical constants for elastic medium (granite) as [27]:

$$\begin{aligned} \lambda^e = 0.884 \times 10^{10} \text{ N/m}^2, \quad \mu^e = 1.2667 \times 10^{10} \text{ N/m}^2, \quad \rho^e = 2.6 \times 10^3 \text{ kg/m}^3, \quad c_e^e = 720.7 \text{ J/kg} \cdot \text{k}, \\ k^e = 3.1 \text{ J/m} \cdot \text{s} \cdot \text{k}. \end{aligned}$$

In light of the results of this paper, the computations are conducted for the value of non-dimensional time $t = 0.01$, in the range of $0 \leq z \leq 0.4$ on the surface $x = 3.01$. The numerical strategy stated herein is utilized for the distribution of horizontal displacement u_1 , the vertical displacement u_3 , the temperature T , the micro-elongational scalar φ , the stress components σ_{xx} , σ_{zz} and σ_{xz} with distance z . To study the influence of rotation on the solution in the DPL model and the L-S theory and the effect of phase-lag of heat flux and phase-lag of temperature gradient on the solution in the DPL model, this paper introduces the results of the numerical assessment in the form of graphs. The results are shown in Figs. 2-15 for the mechanical force with magnitude $P_1 = 1$ for the DPL model and the L-S theory.

5.1. Influence of rotation

Figs. 2-8 show comparison between the displacement components u_1 , u_3 , the temperature T , the micro-elongational scalar φ and the force stresses components σ_{xx} , σ_{zz} , σ_{xz} for various values of Ω ($\Omega = 0.2, 0.5$) for the DPL model and L-S theory. Fig. 2 represents the distribution of the horizontal displacement u_1 with the distance z . It is observed that u_1 increases with the increase of rotation for the two theories. In the DPL model and (L-S) theory, the values of the horizontal displacement u_1 for $\Omega = 0.2$ are small as opposed to those for $\Omega = 0.5$. Fig. 3 illustrates the variation of the vertical displacement u_3 against the distance z , it is observed that the effect of rotation Ω is inversely proportional to the value of the vertical displacement u_3 in the DPL model and L-S theory i.e. the rotation Ω has a decreasing effect. Fig. 4 describes the distribution of the temperature T with the distance z . In this figure, all curves start from a positive value and then converge to zero with large values of the distance z and fulfill the boundary condition. It is obvious that the values of the temperature T increases with increase of rotation for the two theories. Fig. 5 shows the variation of the micro-elongational scalar φ against the distance z , it is clear that the values of φ start from zero and decrease to a minimum then increase up to vanish. It is obvious that the values of φ increase with the decrease of rotation for two theories, and satisfies the boundary condition. Fig. 6 is plotted to describe the distribution of the stress components σ_{xx} with the distance z . In this figure, all curves begin from a positive value, then decrease to a minimum and increase up to vanishes at large values of z . The effect of rotation Ω is directly proportional to the value of the stress component σ_{xx} in both the DPL model and the L-S theory. Fig. 7 exhibits the variation of the stress component σ_{zz} against the distance z . In the DPL model, the effect of different values of rotation is hardly visible. It is shown that the influence of rotation is inversely proportional to the value of the stress component σ_{zz} in the (L-S) theory. Fig 8 compares among the two different values of rotation for the DPL model and the L-S theory. It is obvious that the value of the stress component σ_{xz} increases as the rotation decreasing.

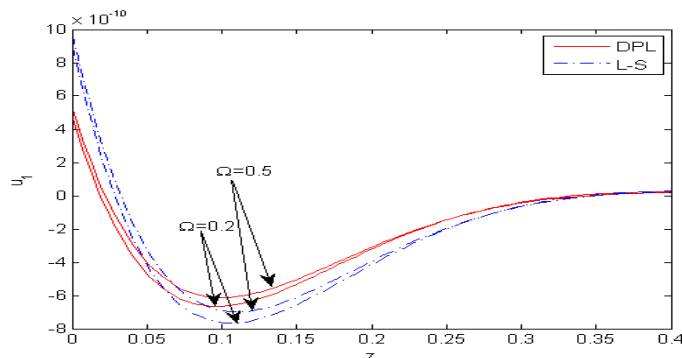


Figure 2. Distribution of the horizontal displacement u_1 with the distance z .

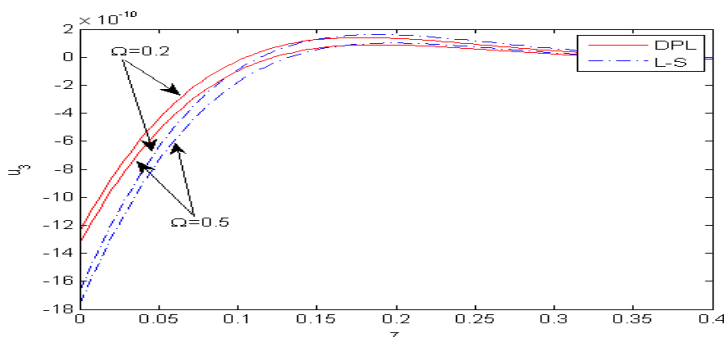


Figure 3. Distribution of the vertical displacement u_3 with the distance z .

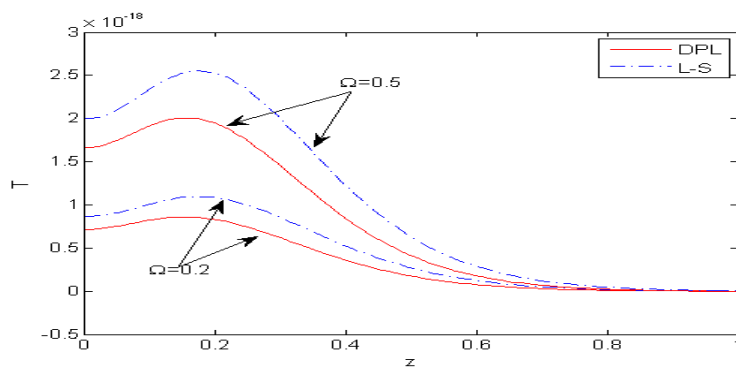


Figure 4. Distribution of the temperature T with distance z .

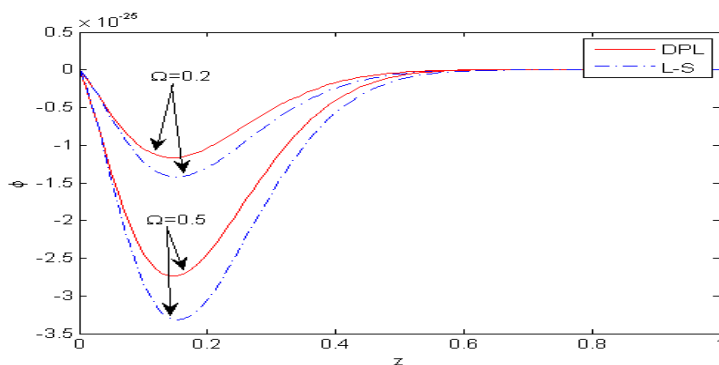


Figure 5. Distribution of the micro-elongational scalar ϕ with the distance z .

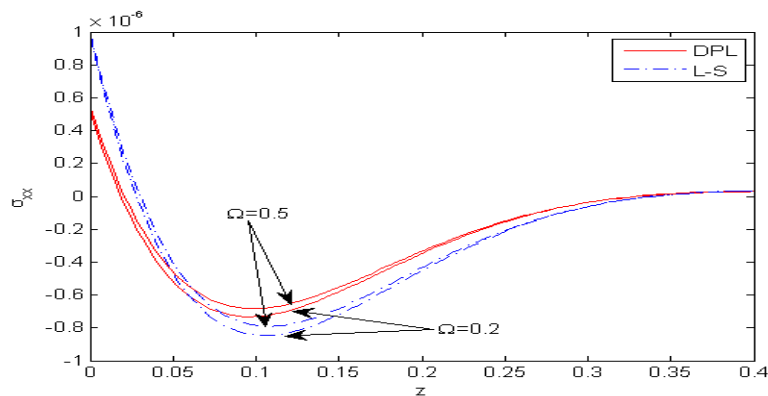


Figure 6. Distribution of the force stress component σ_{xx} with the distance z .

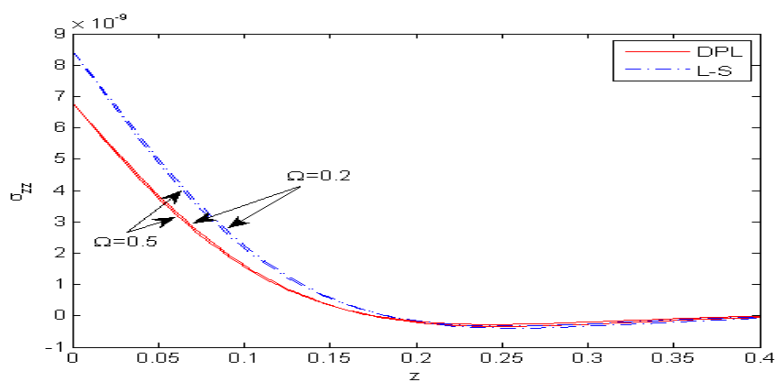


Figure 7. Distribution of the force stress component σ_{zz} with the distance z .

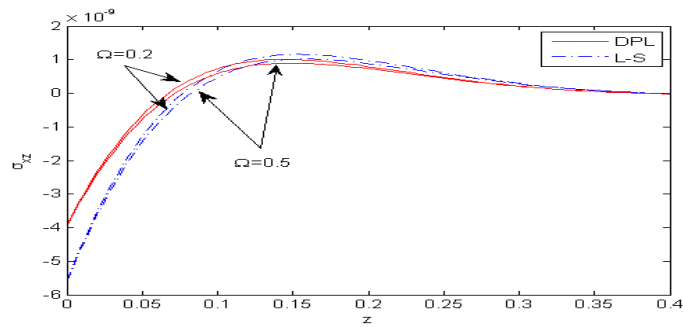


Figure 8. Distribution of the force stress component σ_{xz} with horizontal distance z .

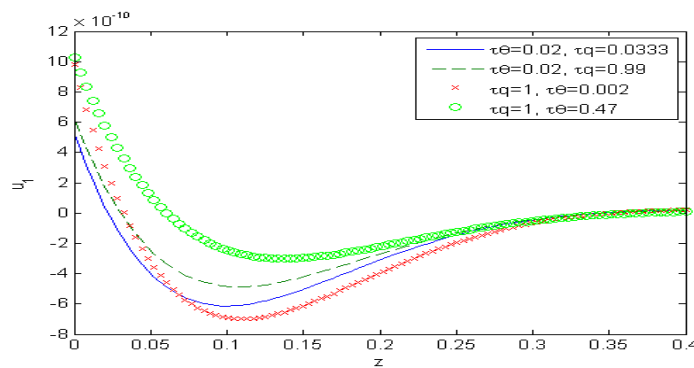


Figure 9. Distribution of the horizontal displacement u_1 with the distance z .

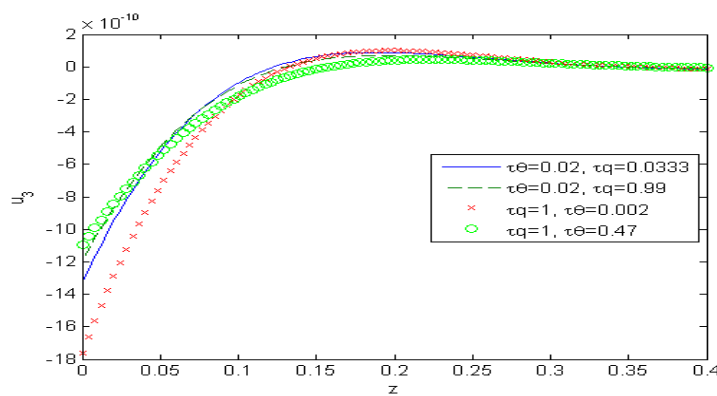


Figure 10. Distribution of the vertical displacement u_3 with the distance z .

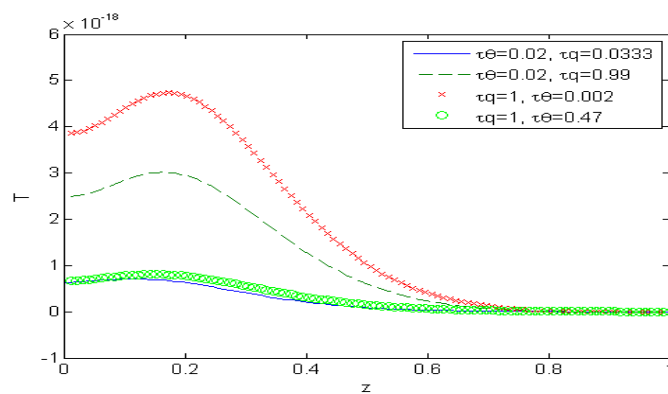


Figure 11. Distribution of the temperature T with distance z .

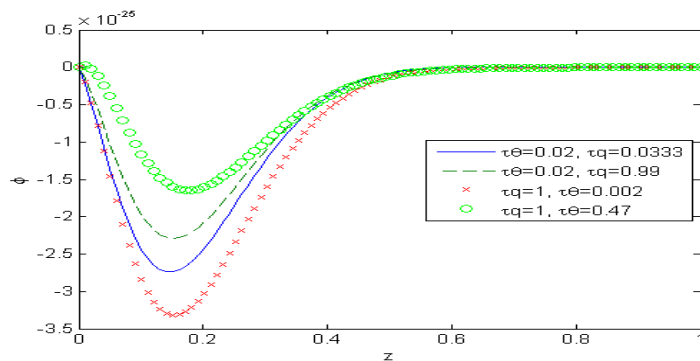


Figure 12. Distribution of the micro-elongational scalar φ with the distance z .

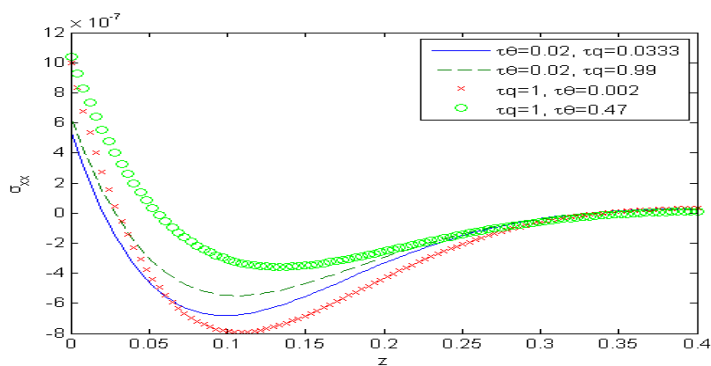


Figure 13. Distribution of the force stress component σ_{xx} with the distance z .

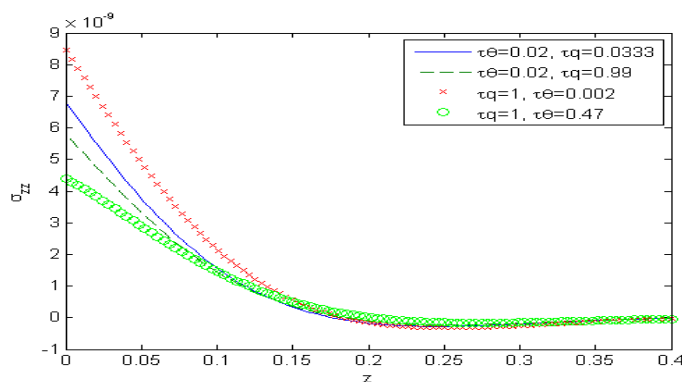


Figure 14. Distribution of the force stress component σ_{zz} with the distance z .

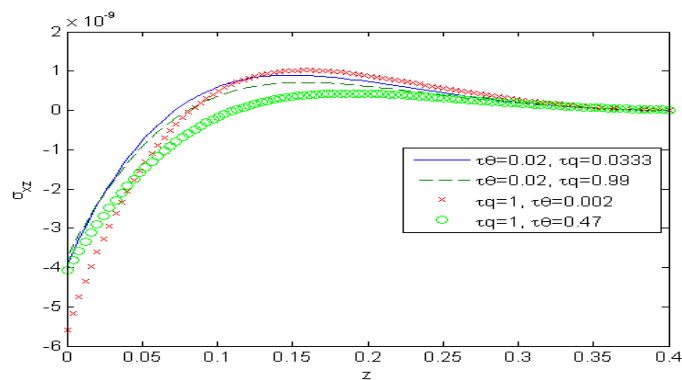


Figure 15. Distribution of the force stress component σ_{xz} with the distance z .

5.2. Influence of the phase-lag of the heat flux and the phase-lag of temperature gradient

Figs. 9-15 show comparison between the displacement components u_1, u_3 , the temperature T , the micro-elongational scalar φ and the force stress components $\sigma_{xx}, \sigma_{zz}, \sigma_{xz}$, when it comes to thermoelasticity the DPL model for different values of the temperature gradient phase-lag τ_θ , such as $\tau_\theta = 0.002, 0.47$ at $\tau_q = 1, \Omega = 0.5$ and for different values of the heat flux phase-lag $\tau_q = 0.0333, 0.99$ at $\tau_\theta = 0.02, \Omega = 0.5$. Fig. 9 depicts that the phase-lag of temperature gradient and the heat flux have an increasing effect on the magnitude of the horizontal displacement u_1 , whereas in Fig. 15, they have a decreasing effect on the magnitude of the stress component σ_{xz} in the range $.05 \leq z \leq 0.4$. Figs. 10 and 13 show that the phase-lag of the heat flux has an increasing effect on the vertical displacement u_3 over the range $0 \leq z \leq 0.11$ and on the stress component σ_{xx} over the range $0 \leq z \leq 0.4$, whereas, the phase-lag of the temperature gradient has a decreasing influence on both. Figs. 11 and 14 in that order, exhibit that the temperature T , and the stress component σ_{zz} are inversely proportional to the value of τ_q for $z > 0$. Fig. 12, explains that the value of micro-elongational scalar φ increases with the increase of τ_q and τ_θ .

5.3. The 3D surface curves

Figs. 16-21 are representing the 3D surface curves for the physical quantities, i.e., the horizontal displacement component u_3 , the micro-elongational scalar φ and the stress components σ_{xx}, σ_{xz} , for the DPL model by keeping in mind the effect of rotation $\Omega = 0.5$. The importance of these figures is that they have been utilized to study the dependence of previous physical quantities on both components of distance.

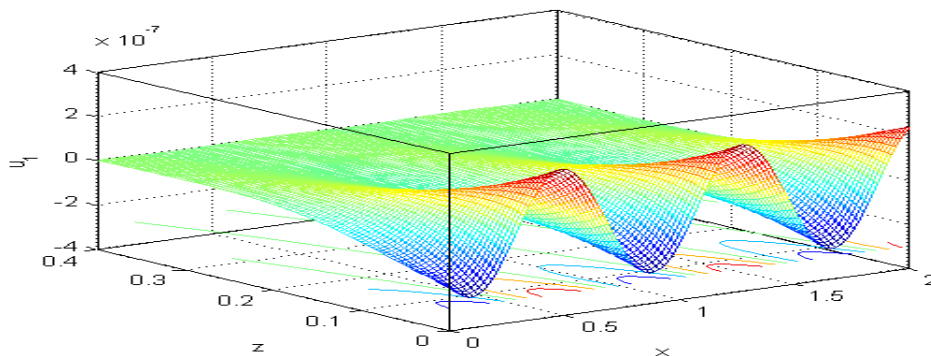


Figure 16. 3D curve distribution of the horizontal displacement u_1 versus distances at $\Omega = 0.5, \tau_\theta = 0.02, \tau_q = 0.5$.

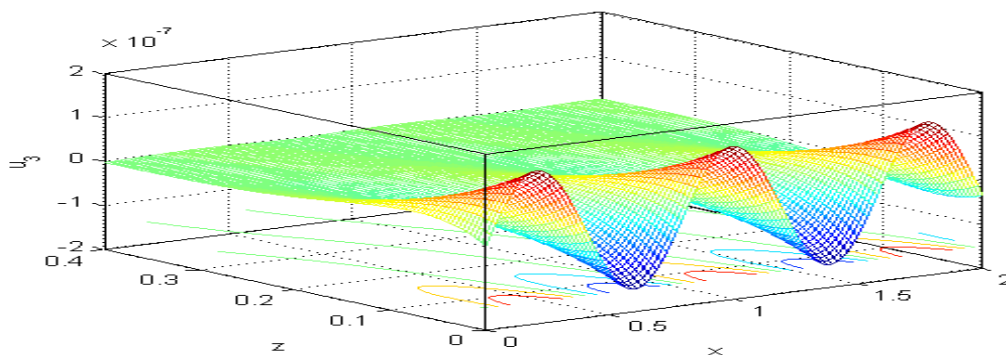


Figure 17. 3D curve distribution of the vertical displacement u_3 versus distances at $\Omega = 0.5, \tau_\theta = 0.02, \tau_q = 0.5$

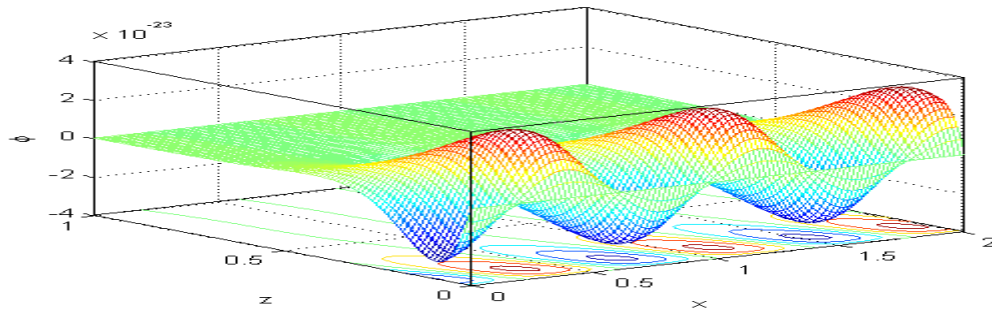


Figure 18. 3D curve distribution of the micro-elongational scalar ϕ versus distances at $\Omega=0.5$, $\tau_\theta=0.02$, $\tau_q=0.5$.

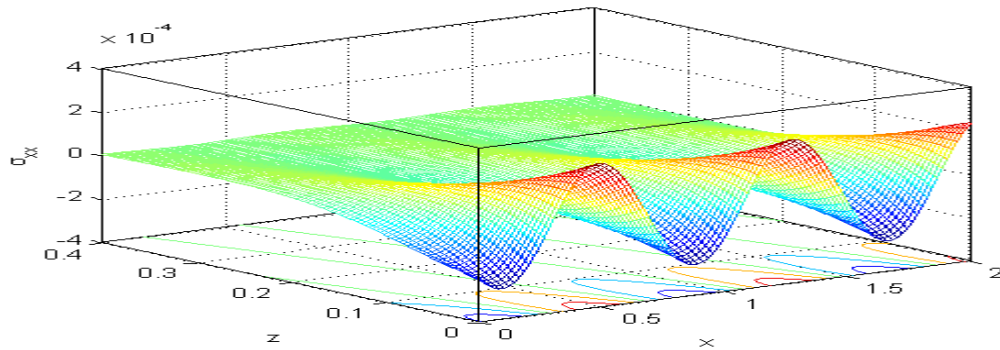


Figure 19. 3D curve distribution of the force stress component σ_{xx} versus distances at $\Omega=0.5$, $\tau_\theta=0.02$, $\tau_q=0.5$.

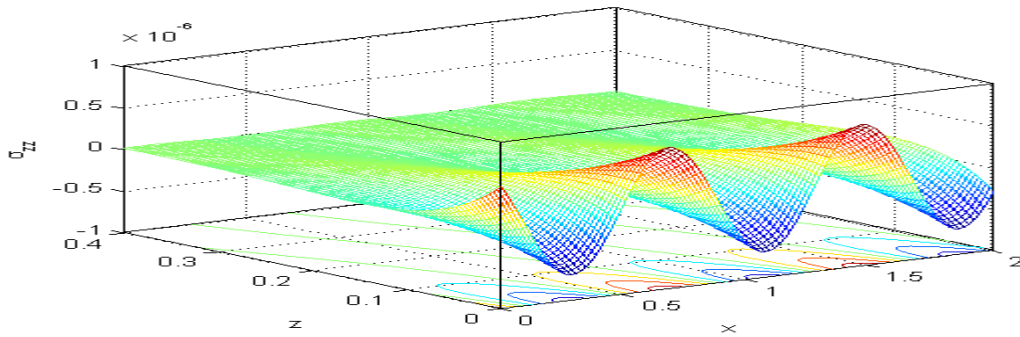


Figure 20. 3D curve distribution of the force stress component σ_{zz} versus distances at $\Omega=0.5$, $\tau_\theta=0.02$, $\tau_q=0.5$.

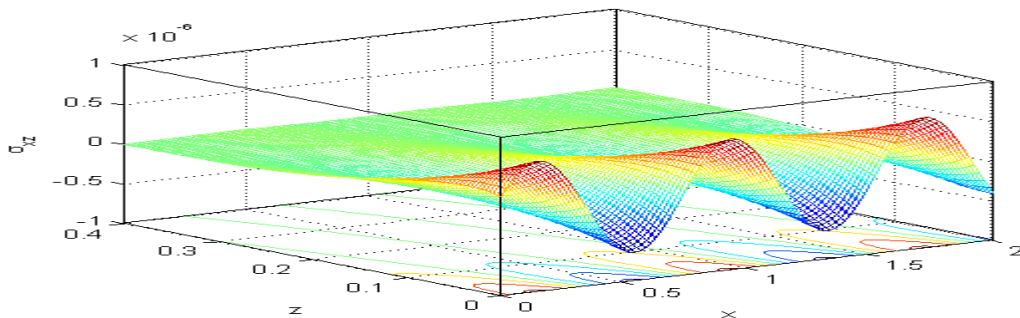


Figure 21. 3D curve distribution of the force stress component σ_{xz} versus distances at $\Omega=0.5$, $\tau_\theta=0.02$, $\tau_q=0.5$.

6. Conclusion

According to the results of this work, one can see that the effect of rotation, the micro-elongational scalar and the applied boundary conditions play a major role in the study of thermoelastic medium deformation. The effect of rotation and the micro-elongational scalar has an obvious influence on all physical quantities. All the physical quantities converge to zero very steeply with the distance z increases. A comparison between the DPL model and the L-S theory is conducted. An analytical solution depended on normal mode analysis of the problem on thermoelastic micro-elongated layer by encircling finite elastic under influence of the rotation has been developed and used it.

Nomenclature

- σ_{ij} Component of stress tensor for micro-elongated medium
- ρ Density in micro-elongated medium
- \mathbf{u} Displacement vector in micro-elongated medium
- Ω Angular velocity
- $a_0, \lambda_0, \lambda_1$ Micro-elongational constants
- $\alpha_{t_1}, \alpha_{t_2}$ Coefficient of linear thermal expansion where $\beta_0 = (3\lambda + 2\mu)\alpha_{t_1}$, $\beta_1 = (3\lambda + 2\mu)\alpha_{t_2}$
- J_0 Microinertia
- φ Micro-elongational scalar
- T Absolute temperature
- T_0 Reference temperature
- k Thermal conductivity in micro-elongated medium
- c_e Specific heat at constant strain in micro-elongated medium
- τ_θ Temperature gradient parameter
- τ_q Heat flux parameter
- λ, μ Lamé's constants in micro-elongated medium
- \mathbf{u}^e Displacement vector in elastic medium
- ρ^e Density in elastic medium
- λ^e, μ^e Lamé's constants in elastic medium
- k^e Thermal conductivity in elastic medium
- c_e^e Specific heat at constant strain in elastic medium

Appendix 1

$$\begin{aligned}
 a_1 &= \frac{\mu}{\rho c_1^2}, \quad a_2 = \frac{\lambda + \mu}{\rho c_1^2}, \quad a_3 = \frac{\beta_1 \lambda_0 c_1^2}{a_0 \beta_0 \omega^{*2}}, \quad a_4 = \frac{\lambda_1 c_1^2}{a_0 \omega^{*2}}, \quad a_5 = \frac{\lambda_0^2}{a_0 \rho \omega^{*2}}, \quad a_6 = \frac{\rho J_0 c_1^2}{2a_0}, \quad a_7 = \frac{\rho c_e c_1^2}{k \omega^{*2}}, \\
 a_8 &= \frac{\beta_0^2 T_0}{k \rho \omega^{*2}}, \quad a_9 = \frac{\beta_1 \beta_0 T_0 c_1^2}{k \lambda_0 \omega^{*2}}, \quad a_{10} = a_1 + a_2, \quad a_{11} = \Omega^2 - \omega^2 - a_{10} b^2, \quad a_{12} = \Omega^2 - \omega^2 - a_1 b^2, \quad a_{13} = a_5 b^2, \\
 a_{14} &= b^2 + a_4 + a_6 \omega^2, \quad a_{14} = b^2 + a_4 + a_6 \omega^2, \quad a_{15} = (1 + \tau_q \omega), \quad a_{16} = (1 + \tau_\theta \omega), \quad a_{17} = a_8 a_{15} \omega, \quad a_{18} = a_8 a_{15} \omega b^2, \\
 a_{19} &= a_{16} b^2 + a_7 a_{15} \omega, \quad a_{20} = \frac{\lambda + 2\mu}{\rho c_1^2}, \quad a_{21} = \frac{\lambda}{\rho c_1^2},
 \end{aligned}$$

$$\begin{aligned}
 A &= \frac{1}{a_1 a_{10} a_{16}} (a_1 a_{17} - a_1 a_5 a_{16} - a_1 a_{11} a_{16} + a_1 a_{10} a_{19} - a_{10} a_{12} a_{16} + a_1 a_{10} a_{14} a_{16}), \\
 B &= \frac{-1}{a_1 a_{10} a_{16}} (-a_1 a_{18} + a_{12} a_{17} - 4a_{16} \omega^2 \Omega^2 + a_1 a_{13} a_{17} + a_1 a_5 a_{19} + a_1 a_{13} a_{16} + a_1 a_{11} a_{19} - a_1 a_{14} a_{17} - a_5 a_{12} a_{16} - a_1 a_{12} a_{16} \\
 &\quad + a_{10} a_{12} a_{19} + a_1 a_{11} a_{14} a_{16} - a_1 a_{10} a_{14} a_{19} + a_{10} a_{12} a_{14} a_{16} + a_1 a_5 a_9 \omega - a_1 a_3 a_9 a_{10} \omega), \\
 C &= \frac{1}{a_1 a_{10} a_{16}} (-a_{12} a_{18} + 4a_{19} \omega^2 \Omega^2 - a_1 a_3 a_{18} + a_3 a_{12} a_{17} - a_1 a_{13} a_{19} + a_1 a_{14} a_{18} + a_5 a_{12} a_{19} + a_{12} a_{13} a_{16} + a_{11} a_{12} a_{19} - a_{12} a_{14} a_{17} \\
 &\quad + 4a_{14} a_{16} \omega^2 \Omega^2 - a_1 a_{11} a_{14} a_{19} + a_{11} a_{12} a_{14} a_{16} - a_{10} a_{12} a_{14} a_{19} - a_1 a_9 a_{13} \omega + a_5 a_9 a_{12} \omega - a_1 a_3 a_9 a_{11} \omega - a_3 a_9 a_{10} a_{12} \omega), \\
 E &= \frac{-1}{a_1 a_{10} a_{16}} (a_{12} a_{14} a_{18} - a_{12} a_{13} a_{19} - a_3 a_{12} a_{18} - 4a_3 a_9 \Omega^2 \omega^3 - 4a_{14} a_{19} \Omega^2 \omega^2 - a_{11} a_{12} a_{14} a_{19} \\
 &\quad - a_9 a_{12} a_{13} \omega - a_3 a_9 a_{11} a_{12} \omega), \\
 H_{2n} &= \frac{-a_{17} k_n^4 + (a_{18} + a_{14} a_{17} - a_5 a_9 \omega) k_n^2 + (a_9 a_{13} \omega - a_{14} a_{18})}{(a_{19} + a_{14} a_{16}) k_n^2 - a_{16} k_n^4 - (a_{14} a_{19} + a_3 a_9)}, \quad H_{3n} = \frac{a_5 k_n^2 - a_{13} - a_3 H_{2n}}{(k_n^2 - a_{14})}, \\
 H_{1n} &= \frac{2\Omega \omega}{a_1 k_n^2 + a_{12}}, \quad H_{4n} = -b^2 a_{20} - i b a_{20} k_n H_{1n} + a_{21} k_n^2 + i b a_{21} k_n H_{1n} - H_{2n} + H_{3n}, \\
 H_{5n} &= a_{20} k_n^2 + i b a_{20} k_n H_{1n} - b^2 a_{21} - i b a_{21} k_n H_{1n} - H_{2n} + H_{3n}, \\
 H_{6n} &= -i b q k_n + a_1 k_n^2 H_{1n} - i b q k_n + a_1 b^2 H_{1n}.
 \end{aligned}$$

Appendix 2

$$\begin{aligned}
 l_1 &= \frac{\lambda^e + 2\mu^e}{\rho^e c_1^{e2}}, \quad l_2 = \frac{\lambda^e + \mu^e}{\rho^e c_1^{e2}}, \quad l_3 = \frac{\mu^e}{\rho^e c_1^{e2}}, \quad l_4 = \frac{\lambda^e}{\rho^e c_1^{e2}}, \quad \delta_1 = b^2 l_1 + \omega^2, \quad \delta_2 = l_3 b^2 + \omega^2, \\
 G &= \frac{b^2 l_2^2 - \delta_1 l_1 - \delta_2 l_3}{l_1 l_3}, \quad N = \frac{\delta_1 \delta_2}{l_1 l_3}, \quad L_{1n} = \frac{l_3 r_n^2 - \delta_1}{i b l_2 r_n}, \quad L_{1(n+2)} = \frac{l_3 r_n^2 - \delta_1}{-i b l_2 r_n}, \quad L_{2n} = i b l_1 - r_n l_4 L_{1n}, \\
 L_{2(n+2)} &= i b l_1 + r_n l_4 L_{1(n+2)}, \quad L_{3n} = i b l_4 - l_1 r_n L_{1n}, \quad L_{3(n+2)} = i b l_4 - l_1 r_n L_{1(n+2)}, \quad L_{4n} = i b l_3 L_{1n} - l_3 r_n, \\
 L_{4(n+2)} &= i b l_3 L_{1(n+2)} + l_3 r_n.
 \end{aligned}$$

References

- [1] Lord, H.W., Shulman, Y. (1967). A generalized dynamical theory of thermo-elasticity. *Journal of the Mechanics and Physics of Solids*, 15:299-306.
- [2] Ezzat, M., Zakaria, M., Shaker, O., Barakat, F. (1996). State space formulation to viscoelastic fluid flow of magneto-hydrodynamic free convection through a porous medium. *Acta Mechanica*, 119:147-16.
- [3] Ezzat, M.A., El-Bary, A.A. (2015). Memory-dependent derivatives theory of thermo-visco-elasticity involving two-temperature. *Journal of Mechanical Science and Technology*, 29:4273-4279.
- [4] Ezzat, M.A., El-Karamany, A.S., El-Bary, A.A. (2016). Modeling of memory-dependent derivative in generalized thermoelasticity. *The European Physical Journal Plus*, 131:372.
- [5] Ezzat, M.A., Youssef, H.M. (2010). Stokes' first problem for an electro-conducting micropolar fluid with thermoelectric properties. *Canadian Journal of Physics*, 88(1):35-48
- [6] Green, A.E., Lindsay, K.A. (1972). Thermoelasticity. *Journal of Elasticity*, 2:1-7.
- [7] Shaw, S., Mukhopadhyay, B. (2012). Periodically varying heat source response in a functionally graded microelongated medium. *Applied Mathematics and Computation*, 218(11):6304-6313.

- [8] Shaw, S., Mukhopadhyay, B. (2013). Moving heat source response in a thermo-elastic micro-elongated solid. *Journal of Engineering Physics and Thermophysics*, 86(3): 716-722.
- [9] Ailawalia, P., Sachdeva, S.K. (2015). Plane strain deformation in thermoelastic micro-elongated solid. *Civil and Environmental Research*, 7(2):92-98.
- [10] Ailawalia, P., Sachdeva, S.K., Pathania, D.S. (2015). Plane strain deformation in a thermoelastic microelongated solid with internal heat source. *International Journal of Applied Mechanics and Engineering*, 20(4):717-731.
- [11] Ailawalia, P., Kumar, S., Pathania, D.S. (2016). Internal heat source in thermoelastic micro-elongated solid under Green-Lindsay theory. *Journal of Theoretical and Applied Mechanics*, 46(2):65-82.
- [12] Ailawalia, P., Sachdeva, S.K., Pathania, D.S. (2019). A two dimensional problem on laser pulse heating in thermoelastic microelongated solid. *Archives of Thermo-dynamics*, 40(2):69-85.
- [13] Ailawalia, P., Singla, A. (2019). A thermoelastic microelongated layer immersed in an infinite fluid and subjected to laser pulse heating. *Mechanics and Mechanical Engineering*, 23(1):233-240.
- [14] Othman, M.I.A., Eraki, E.E.M., Atwa, S.Y., Ismail, M.F. (2021). A thermoelastic micro-elongated layer under the effect of gravity in the context of the dual-phase-lag model. *Journal of Applied Mathematics and Mechanics*, 101:e202100109. DOI: 10.1002/zamm.202100109.
- [15] Othman, M.I.A., Tantawi, R.S., Eraki, E.E.M. (2017). Effect of rotation on a semi conducting medium with two-temperature under L-S theory. *Archives of Thermo-dynamics*, 38(2):101-122.
- [16] Othman, M.I.A., Said, S.M., Marin, M. (2019). A novel model of plane waves of two-temperature fiber-reinforced thermoelastic medium under the effect of gravity with three-phase-lag model. *International Journal of Numerical Methods for Heat and Fluid Flow*, 29(12) 4788-4806.
- [17] Marin, M., Othman, M.I.A., Abbas, I.A. (2015). An extension of the domain of influence theorem for generalized thermoelasticity of anisotropic material with voids. *Journal of Computational and Theoretical Nanoscience*, 12(8), 1594-1598.
- [18] Ozisik, M.N., Tzou, D.Y. (1994). On the wave theory of heat conduction. *Journal of Heat Transfer. (ASME)*, 116: 526-535.
- [19] Tzou, D.Y. (1995). Experimental support for the lagging behaviour in heat propagation. *Journal of Thermophysics and Heat Transfer*, 9(4):686-693.
- [20] Tzou, D.Y. (1995). A unified field approach for heat conduction from macro- to micro-scales. *Journal of Heat Transfer (ASME)*, 117(1):8-16.
- [21] Alharbi, A.M., Abd-Elaziz, E.M., Othman, M.I.A. (2021). Effect of temperature-dependent and internal heat source on a micropolar thermoelastic medium with voids under 3PHL model. *Journal of Applied Mathematics and Mechanics*, 101(6):1-24.
- [22] Abd-Elaziz, E.M., Othman, M.I.A. (2019). Effect of Thomson and thermal loading due to laser pulse in a magneto-thermoelastic porous medium with energy dissipation. *Journal of Applied Mathematics and Mechanics*, 99(8):1-18.
- [23] Othman, M.I.A., Abd-Elaziz, E.M. (2015). The effect of thermal loading due to laser pulse in generalized thermoelastic medium with voids in dual phase lag model. *Journal of Thermal Stresses*, 38(9):1068-1082.
- [24] Ailawalia, P., Budhiraja, S. (2014). Dynamic problem in thermoelastic solid using dual-phase-lag model with internal heat source. *Journal of Mathematical Sciences and Applications*, 2(1): 10-16.
- [25] Othman, M.I.A., Hasona, W.M., Abd-Elaziz, E.M. (2014). Effect of rotation on micropolar generalized thermoelasticity with two-temperatures using a dual-phase-lag model. *Canadian Journal of Physics*, 92(2):149-158.
- [26] Othman, M.I.A., Abd-Elaziz, E.M. (2020). Dual-phase-lag model on micropolar thermoelastic rotating medium under the effect of thermal load due to laser pulse. *Indian Journal of Physics*, 94(7):999-1008.
- [27] Ailawalia, P., Sachdeva, S.K., Pathania, D.S. (2016). Internal heat source in thermo-elastic microelongated solid at an interface under Green Lindsay theory. *Journal of Theoretical and Applied Mechanics*, 46(2):65-82.